Significance of distinct electron-correlation effects in determining the (P,T)-odd electric dipole moment of ^{171}Yb

B. K. Sahoo*

Atomic, Molecular and Optical Physics Division, Physical Research Laboratory, Navrangpura, Ahmedabad 380009, India and State Key Laboratory of Magnetic Resonance and Atomic and Molecular Physics, Wuhan Institute of Physics and Mathematics, Chinese Academy of Sciences, Wuhan 430071, China

Yashpal Singh

Graduate School of EEWS, Korea Advanced Institute of Science and Technology (KAIST), 291 Daehak-ro 34141, Daejeon, South Korea

(Received 9 May 2017; published 29 June 2017)

The parity and time-reversal violating electric dipole moment (EDM) of ^{171}Yb is calculated accounting for the electron-correlation effects over the Dirac-Hartree-Fock method in the relativistic Rayleigh-Schrödinger many-body perturbation theory, with the second- [MBPT(2) method] and third-order [MBPT(3) method] approximations, and two variants of all-order relativistic many-body approaches, in the random phase approximation (RPA) and coupled-cluster (CC) method with singles and doubles (CCSD method) framework. We consider electron-nucleus tensor-pseudotensor (T-PT) and nuclear Schiff moment (NSM) interactions as the predominant sources that induce EDM in a diamagnetic atomic system. Our results from the CCSD method to EDM (d_a) of ^{171}Yb due to the T-PT and NSM interactions are found to be $d_a = 4.85(6) \times 10^{-20} \langle\sigma\rangle C_T$ $|e|$ cm and $d_a = 2.89(4) \times 10^{-17} S/(|e|\ \mathrm{fm}^3)$, respectively, where C_T is the T-PT coupling constant and S is the NSM. These values differ significantly from the earlier calculations. The reason for the same has been attributed to large correlation effects arising through non-RPA type of interactions among the electrons in this atom that are observed by analyzing the differences in the RPA and CCSD results. This has been further scrutinized from the MBPT(2) and MBPT(3) results and their roles have been demonstrated explicitly.

DOI: 10.1103/PhysRevA.95.062514

I. INTRODUCTION

The possible existence of intrinsic electric dipole moments (EDMs) of non-degenerate quantum systems like atoms and molecules can signify for the violations of both parity (P) and time-reversal (T) symmetries (P,T-odd) [1–4]. In the atomic sector, measurements have been performed on the ^{133}Cs, ^{205}Tl, ^{129}Xe, ^{199}Hg, and ^{225}Ra atoms which only give upper bounds to EDMs [5–11]. Owing to the open-shell structure of ^{133}Cs and ^{205}Tl atoms, they are suitable to probe electron EDM (d_e) and electron-nucleus (e-N) P,T-odd pseudoscalar-scalar (PS-S) interactions. However, in recent past experiments on polar molecules with strong internal electric field have provided tremendous improvement on the limits on the d_e and e-N coupling coefficient due to PS-S interactions over the atomic experiments [12,13]. On the other hand, diamagnetic (closed-shell) atoms are better suitable to infer the nuclear Schiff moment (NSM) and the coupling coefficients associated with the e-N tensor-pseudotensor (T-PT) and scalar-pseudoscalar (S-PS) interactions. The NSM originates primarily due to the distorted charge distribution inside the atomic nucleus caused by the P,T-odd interactions among the nucleons or from the EDMs and chromo-EDMs of the up ($\tilde{d}_u$) and down ($\tilde{d}_d$) quarks [1,4]. At the tree level, magnitudes of these P,T-odd interactions are predicted to be tiny in the well-celebrated standard model (SM) of particle physics. However, such P,T-odd effects are enlarged manifold in various extensions of SM, such as multi-Higgs, supersymmetry, left-right symmetric models that are trying to address some of the today's very fundamental issues, such as observation of the finiteness of neutrino masses, reasons for observing the matter-antimatter asymmetry in the universe, the existence of dark matter, etc. [14,15]. Thus, the improved limits on EDMs inferred from the atomic experiments combined with accurate calculations can be very useful to support the validity of these proposed models.

Successively, a variety of progressive experimental techniques have been used to improve the precision of EDM measurements in closed-shell atoms. For example, the use of spin-exchange pumped masers and a ^{3}He comagnetometer by Rosenberry and Chupp yields an upper limit to Xe EDM as $d_a(^{129}\mathrm{Xe}) = 0.7 \pm 3.3(\mathrm{stat}) \pm 0.1(\mathrm{sys}) \times 10^{-27}$ e cm [8]. Currently, new proposals to measure EDM of ^{129}Xe are being made to take advantage of its larger spin relaxation time [16–18]. The proposal by Inoue *et al.* [16] argues utilization of the nuclear spin oscillator technique [19] to carry out measurement of Larmor precession with several orders lower than the available results. In the atoms like ^{223}Rn, large enhancement of the EDM signal is expected owing to its large octupole deformed nucleus [20]. Based on this argument, an experiment to measure the EDM of ^{223}Rn has been under progress [21,22]. So far the most precise atomic EDM measurement has been performed on the ^{199}Hg atom, gradually improving its limit in two successive experiments [9,10], among which the best limit has recently been reported by Graner *et al.* [10]. In the earlier experiment, Griffith *et al.* had used a stack of four cells in such a way that electric fields were being created in opposite directions among two middle cells and zero electric field in the outer two cells. Thus, the signal due to EDM was observed as a difference of the Larmor spin precession frequencies originating from the middle two cells, and combinations of

*bijaya@prl.res.in

these four cells were used to measure the magnetic field. In this approach the EDM of the ^{199}Hg atom was observed as $d_a(^{199}\text{Hg}) = [0.49 \pm 1.29(\text{stat}) \pm 0.76(\text{sys})] \times 10^{29}$ e cm [9]. However, in the recent measurement by Graner *et al.,* fused silica vapor cells containing ^{199}Hg atoms were arranged in a stack with a common magnetic field. Optical pumping was being used to spin-polarize the ^{199}Hg atoms, which was orthogonal to the applied magnetic field, and the Faraday rotation of near-resonant light was observed to determine an electric-field-induced perturbation to the Larmor precession frequency. The improved EDM value inferred from the above precession frequencies was $d_a(^{199}\text{Hg}) = [2.20 \pm 2.75(\text{stat}) \pm 1.48(\text{sys})] \times 10^{30}$ e cm, which translates to an upper limit of $|d_a(^{199}\text{Hg})| < 7.4 \times 10^{30}$ e cm with 95% confidence limit. This corresponds to an improvement of at least an order of magnitude over the previous measurement [10]. In a breakthrough, Parker and co-workers have reported measurement of the EDM of the radioactive element ^{225}Ra atom for the first time [11]. Similar to ^{223}Rn, the EDM signal of ^{225}Ra is also enhanced extraordinarily high due to the octupole deformation in its nucleus [20]. Owing to this fact, even if one could measure the EDM of an ^{225}Ra atom to a couple of orders larger than the ^{199}Hg EDM, it is still advantageous to use this result to extract the required information more reliably. To measure the EDM of the ^{225}Ra atom, a cold-atom technique was developed to detect the spin precession holding the atoms in an optical dipole trap. An upper limit of $|d_a(^{225}\text{Ra})| < 5.0 \times 10^{22}$ e cm with a 95% confidence level was inferred from this measurement.

A number of calculations employing variants of relativistic atomic many-body methods have been carried out in the ^{129}Xe, ^{223}Rn, ^{199}Hg, and ^{225}Ra atoms to evaluate quantities that in combinations with the measurements can give limits on various quantities of fundamental interest (for more detail see a recent review [4]). On comparing EDM results from the latest calculations by the relativistic coupled-cluster (RCC) method with the previously reported values from other less sophisticated approaches, it was observed that results were almost in agreement with each other in the ^{129}Xe [23] and ^{223}Rn [24] atoms. This suggested to us that there are strong cancellations among electron-correlation effects in these atoms from the higher-order effects. However, we had found very large differences in the results from the RCC method with the earlier reported calculations in the ^{199}Hg [25,26] and ^{225}Ra atoms [27]. Although detailed analysis of the reasons for large discrepancies in all those calculations were not given before, we had mentioned briefly how the electron-correlation effects that do not appear through the random phase approximation (RPA) are solely responsible for bringing down the results in the latter mentioned two atoms than the previously estimated values. The other diamagnetic atom that is of current interest to measure EDM is the ^{171}Yb atom [28]. In this proposal, it is suggested to use ^{171}Yb as a comagnetometer and a proxy for measuring EDM of the ^{225}Ra atom. Earlier, the feasibility of measuring EDMs in this atom was being discussed extensively in Refs. [29–32], following which a number of theoretical calculations have also already been performed [33–37]. In view of the above-mentioned substantial discrepancies among the results between different theoretical studies in some of the atoms, it would be of vested interest to perform RCC calculations in the ^{171}Yb atom and compare the obtained results with the previously reported values. Providing reliable calculations for this atom can be very useful to infer limits on various fundamental parameters by combining those values with the measured EDMs of the ^{171}Yb atom from the ongoing experiment when it comes to fruition.

The rest of the paper is organized as follows: In the next section, we briefly discuss the theory of atomic EDMs and present the T-PT and NSM interaction Hamiltonians used for the EDM calculations. Then, we describe our many-body methods and procedures for obtaining atomic wave functions at various levels of approximation. This is followed by discussions of our results and comparison of these values with the previously performed calculations. Unless stated otherwise, we use atomic units (a.u.) throughout this paper.

II. THEORY

The P,T-odd Lagrangian for an electron and nucleon (e-n) pair is given by [2]

$$\mathcal{L}_{e-n}^{\text{PT}} = C_T^{e-n}\varepsilon_{\mu\nu\alpha\beta}\bar{\psi}_e\sigma^{\mu\nu}\psi_e\bar{\psi}_n\sigma^{\alpha\beta}\psi_n + C_P^{e-n}\bar{\psi}_e\psi_e\,\bar{\psi}_n i\gamma_5\psi_n, \tag{1}$$

where $\varepsilon_{\mu\nu\alpha\beta}$ is the Levi-Civita symbol and $\sigma_{\mu\nu} = \frac{i}{2}[\gamma_\mu,\gamma_\nu]$, with γ being the Dirac matrices. The constants C_T^{e-n} and C_P^{e-n} represent couplings associated with the respective T-PT and S-PS e-n interactions. Here, ψ_n and ψ_e are the Dirac wave functions of a nucleon and an electron, respectively. In the nonrelativistic limit, the e-n T-PT interaction Hamiltonian from the above Lagrangian yields [38,39]

$$H_{T-PT}^{e-n} = \frac{G_F}{\sqrt{2}}C_T^{e-n}\bar{\psi}_e\gamma_5\sigma_{\mu\nu}\psi_e\,\bar{\psi}_n\iota\gamma_5\sigma_{\mu\nu}\psi_n, \tag{2}$$

where G_F reads as the Fermi constant. In the atomic scale, the above equation can be further simplified to get the corresponding e-N T-PT interaction Hamiltonian as

$$H_{EDM}^{T-PT} = i\sqrt{2}G_F C_T\sum_e \boldsymbol{\sigma}_N\cdot\boldsymbol{\gamma}_e\rho_N(r_e), \tag{3}$$

with C_T being the e-N T-PT coupling constant, $\sigma_N = \langle\sigma_N\rangle\frac{\mathbf{I}}{I}$ is the Pauli spinor of the nucleus for the nuclear spin I, $\rho_N(r)$ is the nuclear density, and the subscripts N and e represent the respective nucleon and electronic coordinates.

Similarly, the Lagrangian for the P,T-odd pion-nucleon-nucleon (π-n-n) interactions that contribute significantly to the EDMs of the diamagnetic atoms is given by [2]

$$\mathcal{L}_{e-n}^{\pi nn} = \bar{g}_0\bar{\psi}_n\tau^i\psi_n\pi^i + \bar{g}_1\bar{\psi}_n\psi_n\pi^0 + \bar{g}_2(\bar{\psi}_n\tau^i\psi_n\pi^i - 3\bar{\psi}_n\tau^3\psi_n\pi^0), \tag{4}$$

where the couplings $\bar{g}_i$ with the superscript $i = 1, 2, 3$ represent the isospin components. The corresponding e-N interaction Hamiltonian is given by [3,40]

$$H_{EDM}^{NSM} = \frac{3\mathbf{S}\cdot\mathbf{r}}{B_4}\rho_N(r), \tag{5}$$

where $\mathbf{S} = S\frac{\mathbf{I}}{I}$ is the NSM and $B_4 = \int_0^\infty dr r^4\rho_N(r)$. The magnitude of NSM S is given by [41–43]

$$S = g_{\pi nn}\times\left(a_0\bar{g}_{\pi nn}^{(0)} + a_1\bar{g}_{\pi nn}^{(1)} + a_2\bar{g}_{\pi nn}^{(2)}\right), \tag{6}$$

where $g_{\pi nn} \simeq 13.5$ is the CP-even π-n-n coupling constant, a_i are the polarization parameters of the nuclear charge distribution, which can be computed to a reasonable accuracy using the Skyrme effective interactions in the Hartree-Fock-Bogoliubov mean-field method [44], and $\bar{g}^{(i)}_{\pi nn}$s with $i = 1, 2, 3$ represents the isospin components of the CP-odd π-n-n coupling constants. These couplings are related to the chromo-EDMs of up-quark ($\tilde{d}_u$) and down-quark ($\tilde{d}_d$) as $\bar{g}^{(1)}_{\pi nn} \approx 2 \times 10^{-12} \times (\tilde{d}_u - \tilde{d}_d)$ [2,45] and $\bar{g}^{(0)}_{\pi nn}/\bar{g}^{(1)}_{\pi nn} \approx 0.2 \times (\tilde{d}_u + \tilde{d}_d)/(\tilde{d}_u - \tilde{d}_d)$ [2,46], where $\tilde{d}_u$ and $\tilde{d}_d$ are scaled to 10^{-26} e cm. Also, it yields a relation with the quantum chromodynamics (QCD) parameter ($\bar{\theta}$) by $|\bar{g}^{(1)}_{\pi nn}| = 0.018(7)\bar{\theta}$ [46]. From the nuclear calculations, one can obtain $S \simeq (1.9d_n + 0.2d_p)$ fm^2 [47]. Thus, it is necessary to obtain accurate values of C_T and S by combining atomic calculations with the experimental EDM results to infer magnitudes of the above fundamental parameters reliably.

III. METHOD OF CALCULATIONS

The EDM of an atomic system in its ground state is given by

$$d_a = \frac{\langle\Psi_0|D|\Psi_0\rangle}{\langle\Psi_0|\Psi_0\rangle}, \tag{7}$$

where D is the electric dipole (E1) operator and ($|\Psi_0\rangle$) is the ground-state wave function corresponding to the atomic Hamiltonian containing both the electromagnetic and P,T-odd weak interactions. Since atoms are spherically symmetric, we use the spherical polar coordinate system to determine atomic wave functions. In this case, operators are expressed in the form of multiple expansion and parity is treated as a good quantum number. Thus, mixture of parities in the wave functions due to both the electromagnetic and weak interactions are done explicitly when required. For this reason, we evaluate the atomic wave functions first by considering only the electromagnetic interactions where parities of the atomic orbitals are still preserved. Then these wave functions are perturbed to the first order due to the P,T-odd operators, because of which parity mixing among the atomic orbitals is carried out explicitly. This is done by expressing the atomic Hamiltonian as

$$H = H^{at} + \lambda H^{\rm PT}, \tag{8}$$

where H^{at} represents the Hamiltonian part that accounts only for the electromagnetic interactions, and $\lambda H^{\rm PT}$ corresponds to one of the considered P,T-odd Hamiltonians, with λ representing either S or C^T depending upon the undertaken P,T-odd Hamiltonian. In this framework, the atomic wave function $|\Psi_0\rangle$ can be expressed as

$$|\Psi_0\rangle \approx \left|\Psi_0^{(0)}\right\rangle + \lambda\left|\Psi_0^{(1)}\right\rangle, \tag{9}$$

where $|\Psi_0^{(0)}\rangle$ and $|\Psi_0^{(1)}\rangle$ are the wave functions due to H^{at} and its first-order correction due to $\lambda H^{\rm PT}$, respectively. Following this Eq. (7) can be approximated to

$$d_a \simeq \lambda\mathcal{R} = 2\lambda\frac{\left\langle\Psi_0^{(0)}\middle|D\middle|\Psi_0^{(1)}\right\rangle}{\left\langle\Psi_0^{(0)}\middle|\Psi_0^{(0)}\right\rangle}. \tag{10}$$

It is worth mentioning here that one can obtain ground-state E1 polarizability (α_d) of the atomic system by using $\lambda|\Psi_0^{(1)}\rangle$ as the first-order perturbed wave function due to the operator D in Eq. (10). Conventionally, the robustness of a many-body method can be judged by its potential to reproduce experimental results. Though a precise experimental value of α_d for Yb is not available, we still carry out calculations of α_d of the ^{171}Yb atom by employing the considered many-body methods and compare our result with the previously available results from other theoretical studies to get some assurance on the accuracies of our calculated $\mathcal{R}$ values.

In fact, calculating atomic wave functions accurately due to the electromagnetic interactions by allowing only one photon exchange, even in the noncovariant form approximation, is also strenuous owing to the two-body form of the electron-electron interaction potential. We consider the Dirac-Coulomb (DC) Hamiltonian as H^{at} in our calculations. Here, we employ relativistic second-order many-body perturbation theory [MBPT(2)] and third-order many-body perturbation theory [MBPT(3)] in the Rayleigh-Schrödinger approach, and RPA and RCC methods for calculating α_d and $\mathcal{R}$ values. To demonstrate relations among these methods, we discuss the formulation of these methods briefly by starting with the common reference wave function $|\Phi_0\rangle$, which is obtained here using the Dirac-Hartree-Fock (DHF) method, by expressing it as

$$\left|\Psi_0^{(0)}\right\rangle = \Omega^{(0)}|\Phi_0\rangle \tag{11}$$

and

$$\left|\Psi_0^{(1)}\right\rangle = \Omega^{(1)}|\Phi_0\rangle, \tag{12}$$

where $\Omega^{(0)}$ and $\Omega^{(1)}$ are known as wave operators that account for the neglected residual electromagnetic interactions (V_{es}) in the DHF method and V_{es} with the considered weak interactions to first order, respectively.

In the MBPT(n) method, we expand the wave operators as

$$\left|\Psi_0^{(0)}\right\rangle = \sum_k^n \Omega^{(k,0)}|\Phi_0\rangle, \tag{13}$$

where $\Omega^{(k,0)}$ is the wave operator with k and zero orders of V_{es} and $H^{\rm PT}$ perturbations, respectively. The first-order correction to $|\Psi_0^{(0)}\rangle$ due to $H^{\rm PT}$ in the MBPT(n) method is then expressed as

$$\left|\Psi_0^{(1)}\right\rangle = \sum_k^{n-1} \Omega^{(k,1)}|\Phi_0\rangle. \tag{14}$$

Here the first index in the superscript of $\Omega^{(k,1)}$ means k orders of V_{es} and superscript 1 means one order of $H^{\rm PT}$. Amplitudes determining equations for these operators are given elsewhere [4]. This follows the expression to evaluate $\mathcal{R}$ values in the MBPT(2) method as

$$\begin{aligned}\mathcal{R} &\approx 2\langle\Phi_0|[\Omega^{(0,0)} + \Omega^{(1,0)}]^\dagger D[\Omega^{(0,1)} + \Omega^{(1,1)}]|\Phi_0\rangle \\ &\approx 2\langle\Phi_0|D\Omega^{(0,1)} + D\Omega^{(1,1)} + \Omega^{(1,0)^\dagger}D\Omega^{(0,1)} \\ &\quad + \Omega^{(1,0)^\dagger}D\Omega^{(1,1)}|\Phi_0\rangle,\end{aligned} \tag{15}$$

and in the MBPT(3) method as

$$\begin{aligned}\mathcal{R} &\approx 2\langle\Phi_0|[\Omega^{(0,0)}+\Omega^{(1,0)}+\Omega^{(2,0)}]^\dagger D \\ &\quad\times[\Omega^{(0,1)}+\Omega^{(1,1)}+\Omega^{(2,1)}]|\Phi_0\rangle \\ &\approx 2\langle\Phi_0|D\Omega^{(0,1)}+D\Omega^{(1,1)}+D\Omega^{(2,1)}+\Omega^{(1,0)^\dagger}D\Omega^{(0,1)} \\ &\quad+\Omega^{(1,0)^\dagger}D\Omega^{(1,1)}+\Omega^{(2,0)^\dagger}D\Omega^{(0,1)}|\Phi_0\rangle. \end{aligned} \tag{16}$$

Though these approaches are convenient to implement, the number of diagrams increase rapidly from the MBPT(2) to MBPT(3) method (seven to more than 200 diagrams). Thus, it is challenging to go beyond the MBPT(3) method. However, the behavior of various correlation effects can be investigated explicitly through these approximations. Here, we have applied these methods to explain the reasons for the discrepancies between the results obtained using the RPA and RCC methods.

In the RPA, $\mathcal{R}$ values are calculated as

$$\begin{aligned}\mathcal{R} &= 2\langle\Phi_0|\Omega^{(0,0)^\dagger}D\Omega^{(1)}_{RPA}|\Phi_0\rangle \\ &= 2\langle\Phi_0|D\Omega^{(1)}_{RPA}|\Phi_0\rangle, \end{aligned} \tag{17}$$

where the first-order perturbed wave operator is given by

$$\begin{aligned}\Omega^{(1)} &\approx \sum_k^\infty\sum_{p,a}\Omega^{(k,1)}_{p,a} \\ &= \sum_{k=1}^\infty\sum_{pq,ab}\left(\frac{\left[\langle pb|\frac{1}{r_{ij}}|aq\rangle-\langle pb|\frac{1}{r_{ij}}|qa\rangle\right]\Omega^{(k-1,1)}_{b,q}}{\epsilon_p-\epsilon_a}\right. \\ &\quad\left.+\frac{\Omega^{(k,1)^\dagger}_{b,q}\left[\langle pq|\frac{1}{r_{ij}}|ab\rangle-\langle pq|\frac{1}{r_{ij}}|ba\rangle\right]}{\epsilon_p-\epsilon_a}\right), \end{aligned} \tag{18}$$

where the sums over a and p represent replacement of an occupied orbital a by a virtual orbital p in $|\Phi_0\rangle$, corresponding to a class of single excitations. Formulation of the wave operator in this approach encapsulates the core-polarization effects to all orders, which plays dominant roles in determining the investigated properties in this work. In can be noted that it is straightforward to implement RPA and requires much less computational time to obtain the $\mathcal{R}$ values than the MBPT(3) method. Since it is able to capture the electron core-polarization effects to all orders, one would expect to get reasonably accurate values using RPA than the MBPT(2) and MBPT(3) methods.

In the RCC method, we express the unperturbed wave operator as

$$\Omega^{(0)} = e^{T^{(0)}} \tag{19}$$

and the first-order perturbed wave operator as

$$\Omega^{(1)} = e^{T^{(0)}}T^{(1)}, \tag{20}$$

where $T^{(0)}$ and $T^{(1)}$ are referred to as the excitation operators that produce excited-state configurations after operating upon $|\Phi_0\rangle$ due to V_{es} and due to V_{es} along with the perturbed $H^{\rm PT}$ operator, respectively. We have allowed only the the single and double excitations in the RCC method [coupled-cluster (CC) with singles and doubles (CCSD) method approximation] by defining

$$T^{(0)} = T^{(0)}_1 + T^{(0)}_2 \quad\text{and}\quad T^{(1)} = T^{(1)}_1 + T^{(1)}_2, \tag{21}$$

where the subscripts 1 and 2 represent the singly and doubly excited configurations, respectively. The amplitudes determining equations of these RCC excitation operators are described in our previous works [23–25,27]. The CCSD method should give the most accurate results for $\mathcal{R}$ than all the employed methods, as it subsumes contributions arising through the RPA method as well as accounts for other types of correlation effects, such as the electron pair-correlation effects, to all orders which are arising in the MBPT(3) method as the lowest order non-RPA type of contributions. Importantly, all these correlation effects are coupled through the RCC amplitude solving equations as in the natural situation. In this approach,

$$\begin{aligned}\mathcal{R} &= 2\frac{\langle\Phi_0|e^{T^{\dagger(0)}}De^{T^{(0)}}T^{(1)}|\Phi_0\rangle}{\langle\Phi_0|e^{T^{\dagger(0)}}e^{T^{(0)}}|\Phi_0\rangle} \\ &= 2\langle\Phi_0|(\overline{D}^{(0)}T^{(1)})_{\rm con}|\Phi_0\rangle, \end{aligned} \tag{22}$$

where $\overline{D}^{(0)} = e^{T^{\dagger(0)}}De^{T^{(0)}}$ is a nonterminating series. In order to account for most of the contributions from $\overline{D}^{(0)}$ term, we adopt a self-consistent procedure to compute it as explained in our earlier works [25–27,48].

IV. RESULTS AND DISCUSSION

In Table I, we present α_d and $\mathcal{R}$ values due to both the T-PT and NSM interactions in ^{171}Yb by means of the earlier discussed many-body methods and compare them with the previously reported results [33–37]. For convenience, we denote $\mathcal{R}$ values due to the T-PT and NSM interactions as $\mathcal{R}_T$ and $\mathcal{R}_S$, respectively. As can be seen, the DHF value of α_d and the CCSD result differ marginally, giving an impression that the roles of the electron-correlation effects in the evaluation of atomic wave functions in this atom are not very strong. However, analyzing results for this quantity from the MBPT(2), MBPT(3), and RPA methods indicates a different scenario. The MBPT(2) method gives a larger value, while the MBPT(3) method gives a lower value of α_d from the DHF method. The all-order RPA method gives a very large value than all these methods, and the all-order CCSD method brings down this value drastically. It can be noted that the MBPT(2) method possesses all the lowest order core-polarization effects, and the MBPT(3) method accounts for the lowest order correlation effects that do not belong to the core-polarization effects, which are discussed elaborately below. Significant differences between the α_d values from the MBPT(2) and MBPT(3) methods suggest substantial contributions from these other than the core-polarization effects and with the opposite sign than the core-polarization contributions. In the all-order level, differences between the RPA and CCSD results imply net contributions from other than core-polarization effects. A number of calculations on these quantities are also carried out [49–52] employing variants of many-body methods that are mentioned in Table I. Most of these calculations differ noticeably owing to the large electron-correlation effects associated with this atom. We had also obtained this value earlier using the CCSD method, and it was reported as 144.59(5.64) a.u. [50],

TABLE I. Results of $\alpha_d, \mathcal{R}_T$, and $\mathcal{R}_S$, in units of ea_0^3, $(\times 10^{-20}\langle\sigma\rangle|e|\text{cm})$ and $(\times 10^{-17}[1/|e|\text{fm}^3]|e|\text{cm})$ respectively, for the ground state of ^{171}Yb from the employed many-body methods and comparison with the other studies.

Method	α_d	$\mathcal{R}_T$	$\mathcal{R}_S$	Reference
DHF	124.51	−0.71	−0.42	This work
MBPT(2)	141.25	−2.49	−1.42	This work
MBPT(3)	115.70	−2.34	−1.34	This work
RPA	179.76	−3.39	−1.91	This work
CCSD	135.50	−2.04	−1.51	This work
From other works				
DHF		−0.70	−0.42	[34]
RPA	179	−3.4	−1.91	[33,34]
CI + MBPT		−3.70	−2.12	[34]
CI + MBPT + RPA		−3.7	−2.1	[34]
RPA	176.16		−1.903	[35]
MCDF			−2.15	[36]
DHF		−2.51[a]		[37]
PCI		−3.22[a]		[37]
CI + MBPT	111.3(5)			[49]
CCSD[c]	144.59(5.64)			[50]
CCSD(T)	143.1[b]			[51]
CI + all order	141(3)			[52]
Experiment	142(36)			[53]

[a]This is a variational approach. Sign has been changed as per the convention of this work.

[b]Douglas-Kroll-Hess Hamiltonian and effective core-polarization approximation.

[c]Only linear terms of Eq. (22) were considered.

considering only the linear terms of $\overline{D}^{(0)}$ in Eq. (22). We find inclusion of contributions from the nonlinear terms reduces this value, because of which we give a slightly smaller value here. Another calculation in the CCSD method with partial triples effects [CCSD(T) method] is also carried out but considering the Douglas-Kroll-Hess Hamiltonian with effective core-polarization approximation [51]. A preliminary experimental result on α_d of the ground state of Yb has been reported with large uncertainty as 142(36) a.u. [53], and all the calculations are within the error bars of the experimental value. Nevertheless, the present result is in close agreement with most of the theoretical values, and also with the central value of the reported experimental result. From this, we can hope that our CCSD method can also estimate the $\mathcal{R}$ values with reasonable accuracy.

Though both the rank and parity of the E1 operator are same as with the considered P,T-odd interaction operators, it can be clearly seen from Table I that the trends of electron-correlation effects in the evaluation of the α_d and $\mathcal{R}$ values are completely different in these properties. The CCSD results for $\mathcal{R}$ are almost 3 times larger than their corresponding DHF values. However, the values obtained in the MBPT(2) method are larger than the CCSD results, and the MBPT(3) values are smaller than the MBPT(2) results. The RPA method in these cases also gives very large values as compared to the CCSD results. One can notice that the electron-correlation effects in the evaluation of $\mathcal{R}_T$ and $\mathcal{R}_S$ are also somewhat different. The

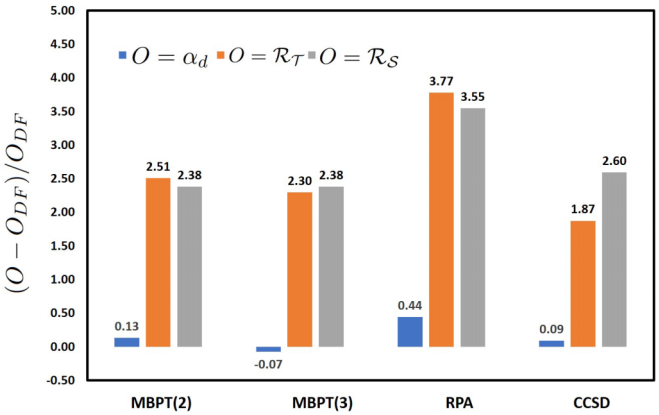

FIG. 1. Comparison of electron-correlation contributions to α_d, $\mathcal{R}_T$, and $\mathcal{R}_S$ in ^{171}Yb at different levels of approximations in the many-body methods with respect to the DHF results. No scaling has been maintained in the x axis, while results plotted in the y axis are unitless.

CCSD value for $\mathcal{R}_T$ is smaller than the MBPT values, while it is larger in case of the NSM interaction. In Fig. 1, we plot the $(O - O_{DF})/O_{DF}$ contributions to α_d and $\mathcal{R}$ values, with O representing values from different many-body methods, which highlights the amount of electron effects that are being accounted for in the evaluation of these quantities through the respective methods. This clearly demonstrates that the electron-correlation effects play vital roles in determining the $\mathcal{R}$ values, more than the α_d result. A few earlier calculations on $\mathcal{R}$ are available using the perturbed configuration interaction (PCI) method [37], RPA [33–35], multiconfiguration Dirac-Fock (MCDF) method [36], and a combined configuration interaction and MBPT (CI + MBPT) method, along with corrections from RPA (CI + MBPT + RPA method) [34]. Our RPA values agree with the RPA results of Dzuba *et al.* [33] but differ slightly from the RPA values reported by Latha and Amjith [35]. The PCI, RPA, and MCDF methods appear to overestimate the $\mathcal{R}$ values more than the CCSD method. Similar trends of the correlation effects were also observed earlier in ^{199}Hg [25,26] and in ^{225}Ra [27]. This clearly demands employing a potential many-body method to evaluate the $\mathcal{R}$ values with reasonable accuracy so that they can be combined with the future experimental result of the ^{171}Yb atom to infer more reliable limits on the C_T and S values.

After presenting the final results from various many-body methods, we now intend to analyze the roles of the electron-correlation effects in the evaluation of the α_d and $\mathcal{R}$ values through various Goldstone diagrams of the MBPT, RPA, and CCSD methods. In Fig. 2, we show some of the important diagrams belonging to the MBPT(3) method. There are more than 200 diagrams which appear in the MBPT(3) method, but we present here contributions only from the selective diagrams that contribute substantially. The first diagram of Fig. 2 represents the DHF method and diagrams up to Fig. 2(vii) correspond to the MBPT(2) method. Individual contributions from these diagrams to α_d and $\mathcal{R}$ are given in Table II. Some of the nonquoted diagrams also contribute in the similar orders with slightly smaller values, but their contributions are not mentioned explicitly here to avoid a very long table. As can be

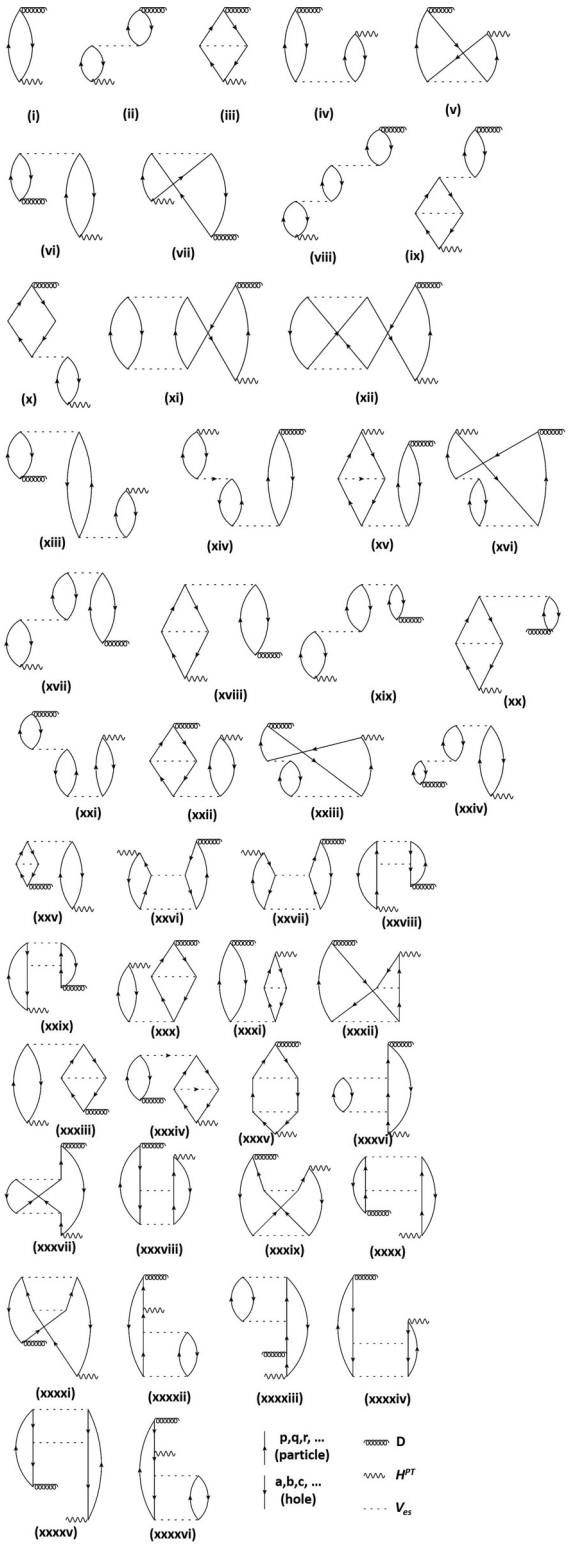

FIG. 2. Important Goldstone diagrams belonging to the MBPT(3) method. Diagram (i) and diagrams up to (vii) correspond to the DHF and MBPT(2) methods, respectively. Operators appearing from right to left in Eqs. (15) and (16) are shown from bottom to top. Lines with arrows up and down represent the virtual and core orbitals, respectively. Symbols for different operators are shown at the end, and the horizontal dashed line corresponds to Coulomb operator.

TABLE II. Explicit contributions to α_d, $\mathcal{R}_T$, and $\mathcal{R}_S$ in units of ea_0^3, $\times 10^{-20}\langle\sigma\rangle|e|$cm and $\times 10^{-17}[1/|e|\text{fm}^3]|e|$cm, respectively, from some of the important Goldstone diagrams of the MBPT(3) method. The first one and along this the next six give DHF and MBPT(2) contributions, respectively.

Diagrams	α_d	$\mathcal{R}_T$	$\mathcal{R}_S$
Fig. 2(i)	124.50	−0.71	−0.42
Fig. 2(ii)	−46.95	−0.02	−0.01
Fig. 2(iii)	92.82	−1.29	−0.72
Fig. 2(iv)	−23.47	−0.41	−0.23
Fig. 2(v)	8.91	−0.29	−0.18
Fig. 2(vi)	−23.47	0.39	0.22
Fig. 2(vii)	8.91	−0.15	−0.08
Fig. 2(viii)	25.03	0.16	0.09
Fig. 2(ix)	−35.26	0.51	0.28
Fig. 2(x)	−35.26	0.03	0.02
Fig. 2(xi)	−31.05	0.42	0.23
Fig. 2(xii)	9.07	−0.11	−0.06
Fig. 2(xiii)	5.11	0.13	0.07
Fig. 2(xiv)	7.69	0.26	0.14
Fig. 2(xv)	−9.09	0.04	0.03
Fig. 2(xvi)	−2.25	0.10	0.06
Fig. 2(xvii)	6.49	−0.12	−0.07
Fig. 2(xviii)	−8.15	0.13	0.07
Fig. 2(xix)	10.85	0.03	0.02
Fig. 2(xx)	−18.02	0.33	0.18
Fig. 2(xxi)	6.49	−0.12	−0.07
Fig. 2(xxii)	−8.15	0.12	0.07
Fig. 2(xxiii)	−2.22	0.10	0.06
Fig. 2(xxiv)	7.69	−0.15	−0.08
Fig. 2(xxv)	−9.09	0.16	0.08
Fig. 2(xxvi)	−8.06	0.14	0.07
Fig. 2(xxvii)	−8.00	0.12	0.06
Fig. 2(xxviii)	−8.09	0.14	0.08
Fig. 2(xxix)	−8.12	0.13	0.07
Fig. 2(xxx)	−8.15	0.12	0.07
Fig. 2(xxxi)	−9.09	0.04	0.03
Fig. 2(xxxii)	3.59	−0.11	−0.07
Fig. 2(xxxiii)	−9.09	0.16	0.08
Fig. 2(xxxiv)	−8.18	0.13	0.07
Fig. 2(xxxv)	70.93	−1.24	−0.67
Fig. 2(xxxvi)	15.72	−0.43	−0.23
Fig. 2(xxxvii)	−3.84	0.10	0.06
Fig. 2(xxxviii)	11.83	−0.17	−0.10
Fig. 2(xxxix)	5.38	−0.11	−0.07
Fig. 2(xxxx)	11.83	−0.20	−0.11
Fig. 2(xxxxi)	5.38	−0.09	−0.05
Fig. 2(xxxxii)	−11.67	−0.25	−0.14
Fig. 2(xxxxiii)	−11.67	−0.04	−0.02
Fig. 2(xxxxiv)	8.91	−0.11	−0.06
Fig. 2(xxxxv)	8.91	−0.14	−0.07
Fig. 2(xxxxvi)	−0.19	−0.10	−0.06

seen from this table, magnitudes and signs of the contributions from various diagrams to α_d and $\mathcal{R}$ with respect to their respective final values exhibit different trends. Contributions from some diagrams to α_d are large, while they contribute less to $\mathcal{R}$. It is also found that some of the individual diagrams

TABLE III. Contributions to α_d, $\mathcal{R}_T$, and $\mathcal{R}_S$ in units of ea_0^3, $\times 10^{-20}\langle\sigma\rangle|e|$cm and $\times 10^{-17}[1/|e|\text{fm}^3]|e|$cm, respectively, from various CCSD terms (Hermitian conjugate terms are included).

CCSD term	α_d	$\mathcal{R}_T$	$\mathcal{R}_S$
$DT_1^{(1)}$	160.55	−2.70	−1.87
$T_1^{(0)\dagger}DT_1^{(1)}$	−11.58	−0.04	−0.01
$T_2^{(0)\dagger}DT_1^{(1)}$	−19.62	0.68	0.41
$T_1^{(0)\dagger}DT_2^{(1)}$	1.06	−0.03	0.02
$T_2^{(0)\dagger}DT_2^{(1)}$	9.05	−0.01	−0.10
Higher	−3.96	0.06	0.04

contribute as large as three-fourths of the total value to α_d. Certain third-order perturbative diagrams also contribute more than the second-order diagrams to this property. Diagrams shown as Fig. 2(xi), 2(xii), 2(xxvi), 2(xxvii), 2(xxix), 2(xxxvi), 2(xxxxii), 2(xxxxiii), 2(xxxxiv), 2(xxxxv), 2(xxxxvi) etc. are some of the dominantly contributing MBPT(3) diagrams that represent results other than the core-polarization effects. These diagrams are solely responsible for bringing down the MBPT(3) values from the results obtained using the MBPT(2) method. They do not appear through the all-order RPA method but appear in the CCSD method to all orders. This is the main reason why the CCSD results are found to be much smaller than the RPA values, as quoted in Table I. Comparing contributions to the $\mathcal{R}$ values from the T-PT and NSM interactions, we find they maintain a scaling among the contributions from each diagram. Contributions to the T-PT result are about 2 times larger than the NSM contributions for the individual diagram. In fact, some of the correlation contributions to α_d are found to have an opposite sign to its DHF value, hence canceling out a large part of the correlation contributions to give the smaller net value. On the contrary, the dominant contributions from the MBPT method to $\mathcal{R}$ have the same sign with their DHF values from the respective P,T-odd interactions. This is why enhancement in the $\mathcal{R}$ values from their DHF values are found to be much larger than the α_d result. It is also found that other than the core polarization, contributions are proportionally larger in the determination of the $\mathcal{R}$ values than the α_d result.

In Table III, we present contributions from the individual CCSD terms. This shows the dominant contributions come from the $DT_1^{(1)}$ term followed by $T_2^{(0)\dagger}DT_1^{(1)}$. Contribution from $T_1^{(0)\dagger}DT_1^{(1)}$ to α_d is also quite large; however its contributions to $\mathcal{R}$ are very small. It can be noticed from Fig. 1 that contributions from most of these diagrams from the MBPT(3) method are accounted for in the $DT_1^{(1)}$ term through the RCC formulation and the rest arise through the $T_2^{(0)\dagger}DT_1^{(1)}$ term. This is the reason why $DT_1^{(1)}$ and $T_2^{(0)\dagger}DT_1^{(1)}$ terms have major shares to the CCSD results, as demonstrated in Table III. In addition to the above, contributions coming through $T_1^{(0)\dagger}DT_1^{(1)}$ are also from the single excitations in the configuration space and contribute significantly to the final results. It can be noticed from the above table that a substantial amount of contributions also come through the $T_2^{(0)\dagger}DT_2^{(1)}$ term. Breakdowns of one of its diagrams into some of the MBPT(3) diagrams are shown in Fig. 3. As seen from this

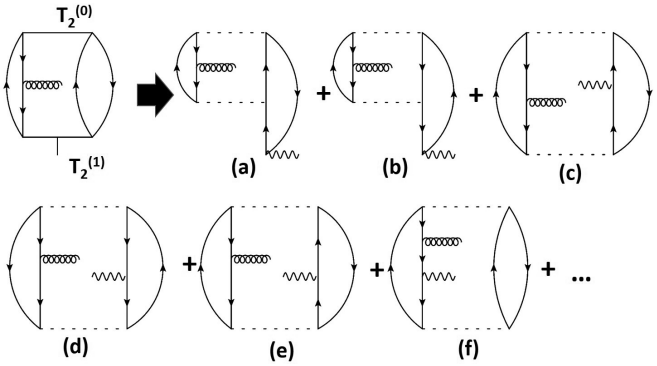

FIG. 3. Breakdown of one of the all-order diagrams representing the $T_2^{(0)\dagger}DT_2^{(1)}$ term is shown explicitly for the comprehensive understanding of how, other correlation effects than the core-polarization correlations are accounted for in the CCSD method for the evaluation of the α_d and $\mathcal{R}$ values.

figure, all the contributions arising through the $T_2^{(0)\dagger}DT_2^{(1)}$ term are due to other than the core-polarization effects, and they are important in determining the α_d value, while they contribute relatively less in the evaluation of the $\mathcal{R}$ values. These MBPT(3) diagrams were not shown explicitly in Fig. 1, as each of these diagrams contribute little, but they add up to a sizable amount in the CCSD method. In the above table, we also quote contributions from the remaining terms of the CCSD method as "higher," because they correspond to higher-order correlation effects and arise through the nonlinear terms such as the $T_1^{(0)\dagger}DT_1^{(0)}T_1^{(1)}$, $T_2^{(0)\dagger}DT_2^{(0)}T_1^{(1)}$, etc. terms. Most of these contributions are due to other than the core-polarization effects.

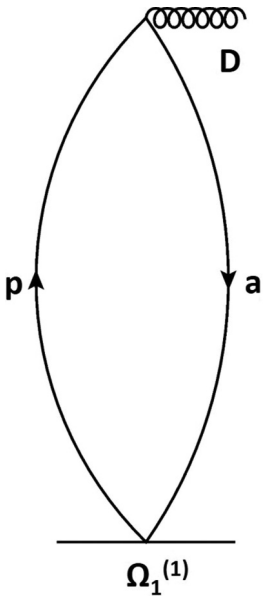

FIG. 4. The Goldstone diagram depicting single excitation contributions to α_d and $\mathcal{R}$ by exciting a core orbital "a" to a virtual orbital "p" through the $\Omega^{(1)}$ operator. Here $\Omega^{(1)}$ represents the first-order perturbed operator in the DHF, MBPT(2), and RPA methods and the $T_1^{(1)}$ operator of the CCSD method.

TABLE IV. Contribution from various atomic orbitals to α_d, $\mathcal{R}_T$, and $\mathcal{R}_S$ in units of ea_0^3, $\times 10^{-20}\langle\sigma\rangle|e|$cm and $\times 10^{-17}[1/|e|\text{fm}^3]|e|$cm, respectively, through dominantly contributing single excitations represented by Fig. 4. Values that are smaller in magnitude are approximated to zero (mentioned as ∼0.0), and those marked in bold fonts highlight changes in the trends of the results from the DHF method after incorporating electron-correlation effects through different many-body methods. Contributions from the 6*s* and $p_{3/2}$ orbitals are quoted within two lines to demonstrate how they behave differently in the evaluation of the α_d and $\mathcal{R}$ values using the considered methods.

Occupied	Virtual	α_d				$\mathcal{R}_T$				$\mathcal{R}_S$			
a	*p*	DHF	MBPT(2)	RPA	$DT_1^{(1)}$	DHF	MBPT(2)	RPA	$DT_1^{(1)}$	DHF	MBPT(2)	RPA	$DT_1^{(1)}$
4*s*	$11p_{1/2}$	∼0.0	∼0.0	∼0.0	∼0.0	0.02	−0.07	0.03	0.03	0.01	−0.02	0.01	0.01
3*s*	$12p_{1/2}$	∼0.0	∼0.0	∼0.0	∼0.0	0.02	−0.04	0.02	0.02	0.01	−0.01	0.01	0.01
4*s*	$12p_{1/2}$	∼0.0	∼0.0	∼0.0	∼0.0	0.05	−0.14	0.05	0.05	0.01	−0.03	0.01	0.01
5*s*	$10p_{1/2}$	∼0.0	∼0.0	∼0.0	∼0.0	0.04	0.09	0.05	0.05	0.01	0.02	0.01	0.01
5*s*	$11p_{1/2}$	∼0.0	∼0.0	∼0.0	∼0.0	0.07	0.01	0.08	0.08	0.02	∼0.0	0.02	0.02
5*s*	$12p_{1/2}$	∼0.0	∼0.0	∼0.0	∼0.0	0.02	−0.06	0.02	0.02	∼0.0	−0.01	0.01	0.01
6*s*	$6p_{1/2}$	9.38	12.39	15.97	11.84	−0.22	−0.29	−0.78	−0.76	−0.05	−0.07	−0.18	−0.16
6*s*	$7p_{1/2}$	22.54	28.94	37.35	29.90	−0.69	−0.88	**−2.32**	**−2.29**	−0.17	−0.21	**−0.54**	**−0.49**
6*s*	$8p_{1/2}$	7.95	8.80	11.37	12.09	−0.52	−0.57	**−1.53**	**−1.59**	−0.12	−0.14	**−0.37**	**−0.35**
6*s*	$9p_{1/2}$	0.20	0.20	0.04	0.36	−0.12	0.05	−0.27	−0.29	−0.03	0.01	−0.07	−0.07
6*s*	$10p_{1/2}$	∼0.0	∼0.0	∼0.0	∼0.0	0.02	0.11	0.03	0.03	∼0.0	0.03	0.01	0.01
6*s*	$6p_{3/2}$	14.01	18.57	23.44	17.54	∼0.0	∼0.0	0.05	0.19	−0.05	−0.07	−0.16	−0.13
6*s*	$7p_{3/2}$	43.44	55.96	**70.39**	57.35	∼0.0	∼0.0	0.17	**0.71**	−0.21	−0.27	**−0.63**	**−0.53**
6*s*	$8p_{3/2}$	18.73	20.99	25.86	28.03	∼0.0	∼0.0	0.06	**0.48**	−0.21	−0.21	**−0.52**	**−0.48**
$5p_{1/2}$	8*s*	∼0.0	∼0.0	∼0.0	∼0.0	0.02	∼0.0	0.02	0.02	∼0.0	∼0.0	0.01	∼0.0
$5p_{1/2}$	9*s*	0.03	∼0.0	−0.03	∼0.0	0.09	−0.02	0.13	0.11	0.02	∼0.0	0.03	0.03
$4p_{1/2}$	10*s*	∼0.0	∼0.0	∼0.0	∼0.0	0.01	−0.02	0.01	0.01	∼0.0	−0.01	∼0.0	∼0.0
$5p_{1/2}$	10*s*	0.03	−0.01	−0.04	∼0.0	0.19	−0.09	**0.26**	**0.24**	0.05	−0.02	**0.07**	**0.06**
$4p_{1/2}$	11*s*	∼0.0	∼0.0	∼0.0	∼0.0	0.04	−0.12	0.04	0.04	0.01	−0.03	0.01	0.01
$5p_{1/2}$	11*s*	∼0.0	∼0.0	∼0.0	∼0.0	0.09	−0.12	0.10	0.10	0.02	−0.03	0.03	0.02
$3p_{1/2}$	12*s*	∼0.0	∼0.0	∼0.0	∼0.0	0.01	−0.02	0.02	0.02	∼0.0	−0.01	∼0.0	∼0.0
$4p_{1/2}$	12*s*	∼0.0	∼0.0	∼0.0	∼0.0	0.03	−0.08	0.03	0.03	0.01	−0.02	0.01	0.01
$5p_{3/2}$	8*s*	0.03	∼0.0	−0.03	0.01	∼0.0	∼0.0	∼0.0	∼0.0	0.01	∼0.0	0.01	0.01
$5p_{3/2}$	9*s*	0.11	−0.03	−0.13	0.02	∼0.0	∼0.0	0.02	0.01	0.04	−0.01	0.07	0.06
$4p_{3/2}$	10*s*	∼0.0	∼0.0	∼*D*0.0	∼0.0	∼0.0	∼0.0	∼0.0	∼0.0	0.01	−0.01	0.01	0.01
$5p_{3/2}$	10*s*	0.10	−0.06	−0.13	∼0.0	∼0.0	∼0.0	0.03	0.02	0.08	−0.05	**0.12**	**0.11**
$4p_{3/2}$	11*s*	∼0.0	∼0.0	∼0.0	∼0.0	∼0.0	∼0.0	∼0.0	∼0.0	0.02	−0.05	0.01	0.02
$5p_{3/2}$	11*s*	∼0.0	−0.01	∼0.0	∼0.0	∼0.0	∼0.0	∼0.0	∼0.0	0.03	−0.05	0.03	0.04
$3p_{3/2}$	12*s*	∼0.0	∼0.0	∼0.0	∼0.0	∼0.0	∼0.0	∼0.0	∼0.0	0.01	−0.01	∼0.0	0.01
$4p_{3/2}$	12*s*	∼0.0	∼0.0	∼0.0	∼0.0	∼0.0	∼0.0	∼0.0	∼0.0	0.01	−0.03	0.01	0.01
$5p_{3/2}$	12*s*	∼0.0	∼0.0	∼0.0	∼0.0	∼0.0	∼0.0	∼0.0	∼0.0	∼0.0	−0.01	∼0.0	∼0.0

The Goldstone diagram depicting the $D\Omega^{(1)}$ term with the approximation for $\Omega^{(1)}$ as the first-order perturbed operator in the DHF, MBPT(2), and RPA methods and the $T_1^{(1)}$ operator of the CCSD method is shown in Fig. 4. This represents the dominantly contributing singly excited configurations, which we have represented by replacing a core orbital (a), denoted with a line pointing down arrow, by a virtual orbital (p), denoted with a line with upward arrow, at various levels of approximations. Contributions from this diagram at the DHF, MBPT(2), RPA, and CCSD level are listed in Table IV only from the large contributing orbitals. As can be seen from this table, contributions from various orbitals to α_d and $\mathcal{R}$ values are different. In the determination of α_d, only the 6*s* and $p_{1/2,3/2}$ orbitals play all the roles. This trend also shows why and how the RPA result for α_d becomes very large, particularly through the $6s - 7p_{3/2}$ orbitals. It exhibits that the core-polarization effects are changing contributions from these orbitals very strongly at the MBPT(2) and RPA level of approximations, while other types of correlation effects coming through the $DT_1^{(1)}$ RCC term revamp these orbitals further to bring these values down. It can also be seen that the $6s - p_{3/2}$ orbitals contribute more than the $6s - p_{1/2}$ orbitals to this quantity. Comparing with the α_d results, the correlation effects affect the atomic orbitals more strongly in the evaluation of the $\mathcal{R}$ values. Again, the $6s - p_{1/2}$ orbitals contribute more predominantly in the evaluation of $\mathcal{R}$ than the $6s - p_{3/2}$ orbitals. In fact, contributions from the $6s - p_{3/2}$ to these quantities at the DHF values are negligibly small, and other than the core-polarization effects through the $DT_1^{(1)}$ RCC term modified these orbitals drastically to give quite significant contributions to the final results. To highlight the same, results only from the $6s - p_{3/2}$ orbitals are put in between two lines of the table. It can also be noticed that the 6*s* and $p_{1/2,3/2}$ orbitals contribute differently to the $\mathcal{R}_T$ and $\mathcal{R}_S$ values at various levels of approximations in the many-body methods. In contrast to the α_d value, some of the high-lying orbitals also contribute

substantially to these quantities, as these continuums have large overlap over the nuclear region. We have marked in bold fonts some of the quoted contributions from a few specific orbitals to bring into notice how the electron-correlation effects modify these orbitals unusually large in ^{171}Yb for studying atomic properties. This implies that it is important to consider a potential many-body method to determine the $\mathcal{R}$ values in this atom. It also suggests that testing accuracies of the α_d value cannot justify accuracies of the $\mathcal{R}$ values absolutely, but it can only assure the validity of the calculations to some extent.

V. CONCLUSION

The roles of electron-correlation effects in the determination of dipole polarizability and electric dipole moments due to parity and time-reversal symmetry violations considering the tensor-pseudotensor interactions between the electrons with the nucleus and electrons with the nuclear Schiff moment in the ^{171}Yb atom are analyzed. For this purpose, relativistic many-body methods over the Dirac-Hartree-Fock wave function at the approximations of the second- and third-order many-body perturbation theories, random phase approximation, and coupled-cluster method with single and double excitations are employed. Contributions from the core-polarization effects and other possible correlation interactions are investigated categorically from the differences of the random phase approximation and coupled-cluster calculations. To fathom the origin of these differences, contributions in terms of the important Goldstone diagrams appearing through the second-order and third-order perturbative methods are given. Moreover, contributions from different orbitals at various levels of approximations in the many-body methods are listed for the comprehensive understanding of propagation of the electron-correlation effects in the above atom through these orbitals to the considered properties that have distinct radial behaviors. This suggests that accuracies in the calculated electric dipole moments in atoms cannot really be determined from the dipole polarizability calculations. On the grounds of physical effects that are being embodied in the calculations, the values obtained employing our coupled-cluster method can be treated as more accurate, and they can be used to infer reliable limits on the tensor-pseudotensor coupling constant between the electrons and nucleus and nuclear Schiff moment of the ^{171}Yb atom when its experiment comes to fruition.

ACKNOWLEDGMENTS

B.K.S. acknowledges financial support from CAS through the PIFI fellowship under Project No. 2017VMB0023. This work was partly supported by the TDP project of Physical Research Laboratory (PRL), Ahmedabad, and the computations were carried out using the Vikram-100 HPC cluster of PRL.

[1] I. B. Khriplovich and S. K. Lamoreaux, *CP Violation Without Strangeness* (Springer, Berlin, 1997).
[2] M. Pospelov and A. Ritz, Ann. Phys. (NY) **318**, 119 (2005).
[3] V. A. Dzuba and V. V. Flambaum, Int. J. Mod. Phys. E **21**, 1230010 (2012).
[4] N. Yamanaka, B. K. Sahoo, N. Yoshinaga, T. Sato, K. Asahi, and B. P. Das, Eur. Phys. J. A **53**, 54 (2017).
[5] S. A. Murthy, D. Krause, Jr., Z. L. Li, and L. R. Hunter, Phys. Rev. Lett. **63**, 965 (1989).
[6] C. Chin, V. Leiber, V. Vuletić, A. J. Kerman, and S. Chu, Phys. Rev. A **63**, 033401 (2001).
[7] B. C. Regan, E. D. Commins, C. J. Schmidt, and D. DeMille, Phys. Rev. Lett. **88**, 071805 (2002).
[8] M. A. Rosenberry and T. E. Chupp, Phys. Rev. Lett. **86**, 22 (2001).
[9] W. C. Griffith, M. D. Swallows, T. H. Loftus, M. V. Romalis, B. R. Heckel, and E. N. Fortson, Phys. Rev. Lett. **102**, 101601 (2009).
[10] B. Graner, Y. Chen, E. G. Lindahl, and B. R. Heckel, Phys. Rev. Lett. **116**, 161601 (2016).
[11] R. H. Parker, M. R. Dietrich, M. R. Kalita, N. D. Lemke, K. G. Bailey, M. Bishof, J. P. Greene, R. J. Holt, W. Korsch, Z. T. Lu, P. Mueller, T. P. OConnor, and J. T. Singh, Phys. Rev. Lett. **114**, 233002 (2015).
[12] J. J. Hudson, D. M. Kara, I. J. Smallman, B. E. Sauer, M. R. Tarbutt, and E. A. Hinds, Nature (London) **473**, 493 (2011).
[13] The ACME Collaboration, J. Baron, W. C. Campbell, D. DeMille, J. M. Doyle, G. Gabrielse, Y. V. Gurevich, P. W. Hess, N. R. Hutzler, E. Kirilov, I. Kozyryev, B. R. O'Leary, C. D. Panda, M. F. Parsons, E. S. Petrik, B. Spaun, A. C. Vutha, and A. D. West, Science **343**, 269 (2014).
[14] M. Dine and A. Kusenko, Rev. Mod. Phys. **76**, 1 (2003).
[15] L. Canetti, M. Drewes, and M. Shaposhnikov, New J. Phys. **14**, 095012 (2012).
[16] T. Inoue, T. Furukawa, A. Yoshimi, Y. Ichikawa, M. Chikamori, Y. Ohtomo, M. Tsuchiya, N. Yoshida, H. Shirai, M. Uchida, K. Suzuki, T. Nanao, H. Miyatake, H. Ueno, Y. Matsuo, T. Fukuyama, and K. Asahi, Hyperfine Interact. **220**, 59 (2013).
[17] F. Kuchler, E. Babcock, M. Burghoff, T. Chupp, S. Degenkolb, I. Fan, P. Fierlinger, F. Gong, E. Kraegeloh, W. Kilian, S. Knappe-Grüneberg, T. Lins, M. Marino, J. Meinel, B. Niessen, N. Sachdeva, Z. Salhi, A. Schnabel, F. Seifert, J. Singh, S. Stuiber, L. Trahms, and J. Voigt, Hyperfine Interact. **237**, 95 (2016).
[18] W. Heil, C. Gemmel, S. Karpuk, Y. Sobolev, K. Tullney, F. Allmendinger, U. Schmidt, M. Burghoff, W. Kilian, S. Knappe-Grüneberg, A. Schnabel, F. Seifert, and L. Trahms, Ann. Phys. (Berlin, Ger.) **525**, 539 (2013).
[19] A. Yoshimi, K. Asahi, K. Sakai, M. Tsuda, K. Yogo, H. Ogawa, T. Suzuki, and M. Nagakura, Phys. Lett. A **304**, 13 (2002).
[20] N. Auerbach, V. V. Flambaum, and V. Spevak, Phys. Rev. Lett. **76**, 4316 (1996).
[21] E. T. Rand, J. C. Bangay, L. Bianco, R. Dunlop, P. Finlay, P. E. Garrett, K. G. Leach, A. A. Phillips, C. S. Sumithrarachchi, C. E. Svensson, and J. Wong, J. Phys.: Conf. Ser. **312**, 102013 (2011).
[22] E. R. Tardiff, E. T. Rand, G. C. Ball, T. E. Chupp, A. B. Garnsworthy, P. Garrett, M. E. Hayden, C. A. Kierans, W. Lorenzon, M. R. Pearson, C. Schaub, and C. E. Svensson, Hyperfine Interact. **225**, 197 (2014).

[23] Y. Singh, B. K. Sahoo, and B. P. Das, Phys. Rev. A **89**, 030502(R) (2014).
[24] B. K. Sahoo, Y. Singh, and B. P. Das, Phys. Rev. A **90**, 050501(R) (2014).
[25] Y. Singh and B. K. Sahoo, Phys. Rev. A **91**, 030501(R) (2015).
[26] B. K. Sahoo, Phys. Rev. D **95**, 013002 (2017).
[27] Y. Singh and B. K. Sahoo, Phys. Rev. A **92**, 022502 (2015).
[28] T. Xia, M. Dietrich, and Z.-T. Lu (unpublished).
[29] Y. Takahashi, M. Fujimoto, T. Yabuzaki, A. D. Singh, M. K. Samal, and B. P. Das, Electric dipole moment of atomic ytterbium by laser cooling and trapping, in *Proceedings of CP Violation and its Origin*, edited by K. Hagiwara (KEK Report, Tsukuba 1997), p. 259.
[30] M. V. Romalis and E. N. Fortson, Phys. Rev. A **59**, 4547 (1999).
[31] V. Natarajan, Eur. Phys. J. D **32**, 33 (2005).
[32] T. Takano, M. Fuyama, H. Yamamoto, and Y. Takahashi (unpublished).
[33] V. A. Dzuba, V. V. Flambaum, and J. S. M. Ginges, Phys. Rev. A **76**, 034501 (2007).
[34] V. A. Dzuba, V. V. Flambaum, and S. G. Porsev, Phys. Rev. A **80**, 032120 (2009).
[35] K. V. P. Latha and P. R. Amjith, Phys. Rev. A **87**, 022509 (2013).
[36] L. Radžiūtė, G. Gaigalas, P. Jönsson, and J. Bieroń, Phys. Rev. A **90**, 012528 (2014).
[37] A. D. Singh, B. P. Das, W. F. Perger, M. K. Samal, and K. P. Geetha, J. Phys. B: At., Mol. Opt. Phys. **34**, 3089 (2001).
[38] S. M. Barr, Phys. Rev. D **45**, 4148 (1992).
[39] A.-M. Maartensson-Pendrill, Phys. Rev. Lett. **54**, 1153 (1985).
[40] V. V. Flambaum and J. S. M. Ginges, Phys. Rev. A **65**, 032113 (2002).
[41] W. C. Haxton and E. M. Henley, Phys. Rev. Lett. **51**, 1937 (1983).
[42] S. Ban, J. Dobaczewski, J. Engel, and A. Shukla, Phys. Rev. C **82**, 015501 (2010).
[43] J. H. de Jesus and J. Engel, Phys. Rev. C **72**, 045503 (2005).
[44] J. Engel, M. J. Ramsey-Musolf, and U. van Kolck, Prog. Part. Nucl. Phys. **71**, 21 (2013).
[45] M. Pospelov, Phys. Lett. B **530**, 123 (2002).
[46] W. Dekens, J. de Vries, J. Bsaisou, W. Bernreuther, C. Hanhart, Ulf-G. Meißner, A. Nogga, and A. Wirzba, J. High Energy Phys. 07 (2014) 069.
[47] V. F. Dmitriev and R. A. Senkov, Phys. Rev. Lett. **91**, 212303 (2003).
[48] Y. Singh, B. K. Sahoo, and B. P. Das, Phys. Rev. A **88**, 062504 (2013).
[49] S. G. Porsev and A. Derevianko, Phys. Rev. A **74**, 020502(R) (2006).
[50] B. K. Sahoo and B. P. Das, Phys. Rev. A **77**, 062516 (2008).
[51] P. Zhang and A. Dalgarno, J. Phys. Chem. A **111**, 12471 (2007).
[52] M. S. Safronova, S. G. Porsev, and Charles W. Clark, Phys. Rev. Lett. **109**, 230802 (2012).
[53] T. M. Miller, in *CRC Handbook of Chemistry and Physics*, 77th ed., edited by D. R. Lide (CRC Press, Boca Raton, FL, 1996).